Kinematically complete experiment on single ionization in 75-keV p+He collisions

M. Schulz,[1] A. Hasan,[1,2] N. V. Maydanyuk,[1] M. Foster,[1] B. Tooke,[1] and D. H. Madison[1]
[1]*University of Missouri-Rolla, Physics Department and Laboratory for Atomic, Molecular, and Optical Research, Rolla, Missouri 65409, USA*
[2]*Department of Physics, UAE University, P.O. Box 17551, Alain, Abu Dhabi, United Arab Emirates*
(Received 27 March 2006; published 2 June 2006)

We have measured and calculated fully differential single-ionization cross sections for the complete three-dimensional space in 75 keV p+He collisions. Several signatures of the projectile–residual-target-ion interaction, some of which are not observable for fast projectiles and for electron impact, are revealed. Some of these features are qualitatively reproduced by our calculations if this interaction is accounted for. However, overall the agreement between theory and experiment is not very good. Thus, our understanding of effects caused by the projectile–residual-target-ion interaction appears to be rather incomplete.

DOI: 10.1103/PhysRevA.73.062704 PACS number(s): 34.50.Fa, 34.10.+x

I. INTRODUCTION

Kinematically complete experiments—i.e., experiments which determine the momentum vectors of all collision fragments—have been performed for single ionization of neutral atoms by electron impact for nearly 40 years [1,2]. Such studies have proven to be extremely powerful as they yield fully differential cross sections (FDCS's) and therefore provide the most sensitive tests of theoretical models describing few-body dynamics in ionization processes. Generally, theory has been quite successful in reproducing the available experimental data. For high projectile energies and light target atoms perturbative methods usually lead to very good agreement with measured FDCS's [3]. At low projectile energies, even within just a few eV above threshold, nonperturbative calculations reproduce the experimental data very well [4]. Based on these successes it was generally assumed that single ionization of light atoms by charged-particle impact is essentially understood.

This rather optimistic assessment did not account, however, for two important gaps in the available experimental data that existed until very recently. First, the vast majority of experiments were restricted to electrons ejected into the scattering plane (defined by the momentum vectors of the incoming projectile electron and the fast final-state electron). Until data were reported for high-energy electron impact earlier this year [5,6], FDCS's for slow electron ejection outside the scattering plane were only available for relatively small projectile energies [7]. Second, the first measured FDCS's for single ionization by ion impact were only reported about 5 years ago [8]. Although numerous measurements have been performed since then [9,10], the literature on experimental FDCS's for ion impact is not nearly as extensive as for electron impact.

At least for collision systems with small perturbation parameters η (projectile charge to velocity ratio), where higher-order contributions were assumed to be negligible, it was not necessarily expected that the comparison between theory and experiment would be significantly different for electron and ion impact. Indeed, for ion impact at small η the data in the scattering plane were as well reproduced by perturbative calculations as for electron impact [11]. However, in the perpendicular plane, defined by the initial projectile momentum and the vector normal to the scattering plane, surprisingly strong and qualitative discrepancies between the data and a state-of-the-art calculation were found [12]. While the calculation predicted a nearly isotropic behavior in that plane, pronounced maxima perpendicular to the projectile beam direction were observed in the experiment. More recently, similar structures were reported for electron impact at about the same η [5,6].

For fast highly charged ion impact at very large η poor agreement between experiment and theory was obtained even for electrons ejected into the scattering plane [13–17]. Here, the most prominent feature not reproduced by the calculations was a strong peak structure in the forward (initial beam) direction. This maximum, as well as the peak structures found in the perpendicular plane for small η, has been traced to higher-order contributions involving an interaction between the projectile and residual-target-ion interaction (PI interaction) [18]. Although such contributions are conceptually accounted for by theory, their description is apparently incomplete.

More recently, we reported another unexpected effect due to the PI interaction which we found for relatively slow 75-keV p+He collisions [19]. Usually, the so-called binary peak is observed in the FDCS's for the scattering plane in the direction of the momentum transfer vector $\mathbf{q}$ (difference between the initial and scattered projectile momentum). However, for increasing η the binary peak tends to shift in the backward direction relative to $\mathbf{q}$ for the case of electron impact [1] and in the forward direction for ion impact [13,14]. This shift can be explained in terms of the post-collision interaction (PCI) between the outgoing projectile and the ejected electron occurring after the primary ionizing interaction. For 75-keV p+He we actually observed a backward shift instead of a forward shift, which we also explained in terms of the PI interaction [19]. If this interpretation is correct, this effect is not observable for fast heavy-ion impact or for electron impact.

In the original publication we focused on analyzing and interpreting data in the scattering plane. In this article we extend the discussion to data outside the scattering plane. Furthermore, aspects of data for the scattering plane, only treated briefly or not at all in the original publication, are

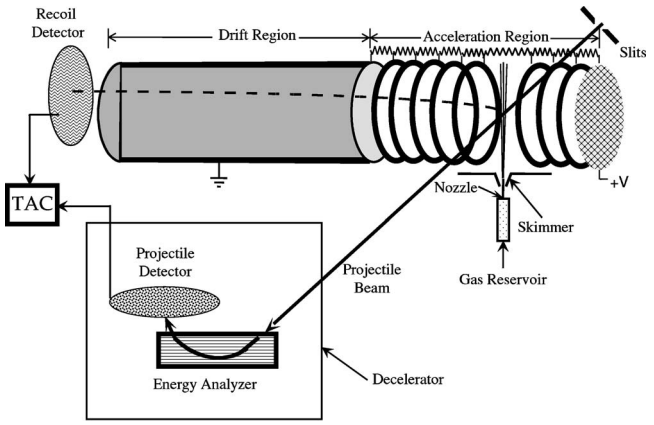

FIG. 1. Schematic diagram of the experimental setup.

analyzed in more detail. Finally, new theoretical calculations are presented.

II. EXPERIMENT

The experiment, which is schematically shown in Fig. 1, was performed at the University of Missouri–Rolla Ion Energy Loss Spectrometer (IELS). A proton beam with an energy of 5 keV and an energy spread of less than 1 eV was produced from a hot cathode ion source and accelerated to an energy of 75 keV. In the target chamber the projectile beam intersected with a very cold ($T<1$ K) neutral helium beam from a supersonic gas jet. A collimator before the target chamber reduced the projectile beam size to approximately 0.1×0.1 mm^2. A switching magnet (not shown in Fig. 1) located after the target chamber separated the different charge states of the projectile. The protons deflected by the magnet were then decelerated to an energy of 5 keV and energy analyzed by an electrostatic parallel plate analyzer [20]. The pass energy of the analyzer corresponded to a projectile energy loss ε of 30 eV, which is equivalent to an ejected electron energy $E_e=\varepsilon-I=5.4$ eV (where I is the ionization potential of He). The energy resolution of the analyzer was ±1.5 eV full width at half maximum (FWHM). Finally, the projectiles were detected by a position-sensitive channel plate detector with a position resolution of ±50 μm FWHM. The entrance and exit slits of the analyzer are long in the x direction ($\approx$2 cm), but very narrow in the y direction ($\approx$75 μm) so that the azimuthal angle of the detected projectiles is kept at 0° and the polar angle θ_p is given by the position information of the detector.

The energy loss can be expressed as

$$\varepsilon = (\mathbf{p}_0-\mathbf{p}_f)^2/2M = (\mathbf{p}_0-\mathbf{p}_f)\cdot(\mathbf{p}_0+\mathbf{p}_f)/2M$$
$$= \mathbf{q}\cdot(\mathbf{p}_0+\mathbf{p}_f)/2M,$$

where $\mathbf{p}_0$ and $\mathbf{p}_f$ are the initial and final projectile momenta and M is its mass. If p_0 is large compared to q and the scattering angle is small, which is always the case for intermediate and fast ion impact, then $\mathbf{p}_0\cong\mathbf{p}_f$ and to a very good approximation $\varepsilon\cong q_z v_p$, where v_p is the projectile speed and q_z is the longitudinal component (z direction) of $\mathbf{q}$. Here $v_p=1.73$ a.u. and $\varepsilon=30$ eV$=1.1$ a.u. so that $q_z=0.638$ a.u. The x component of $\mathbf{q}$ is given by $q_x=p_0\sin\theta_p$ and is obtained from the position information. The y component of q is kept fixed at 0 due to the narrow width of the analyzer slits (see above). The achieved resolutions are ±0.03 a.u. in q_y and q_z and ±0.05 a.u. FWHM in q_x.

The recoil ions were extracted perpendicular to the incident projectile beam by a weak, nearly uniform electric field of 1.6 V/cm. After the electric field region, the recoil ions traveled through a field-free region and were detected by a two-dimensional position-sensitive detector with about the same resolution as the projectile detector. From the position information the y and z components of the recoil-ion momentum could be determined. The x component was obtained from the time of flight from the collision region to the detector, which, in turn, is obtained from the coincidence time spectrum. The main contributor to the resolution is the temperature of the He beam, which mostly affects the y direction. Here, the achieved resolution is ±0.1 a.u. while in the x and z directions it is ±0.075 a.u. The electron momentum is determined from momentum conservation by $\mathbf{p}_e=\mathbf{q}-\mathbf{p}_r$ where $\mathbf{p}_r$ is the final-state momentum of the recoil ion. Due to error propagation in this difference, the resolution in the electron momentum is somewhat worse than in $\mathbf{p}_r$ and $\mathbf{q}$ (about ±0.1 a.u. in all three directions). In magnitude the resolution is significantly better (±0.04 a.u.) because it is only determined by the resolution in ε.

In order to extract the FDCS's from the data, a condition was set on q_x (i.e., the position spectrum of the projectiles). For detected ionization events satisfying this condition the electron momentum was calculated and converted to spherical polar coordinates (p_e, ϕ_e, θ_e), where ϕ_e is the azimuthal angle of the projection of $\mathbf{p}_e$ onto the xy plane relative to the x axis and θ_e is the polar angle of $\mathbf{p}_e$ relative to the initial projectile beam direction (z axis). The three-dimensional angular distribution of the ejected electrons was then generated for the q_x corresponding to the selected condition on the projectile position (since $q_y=0$, q_x is equivalent to the transverse component q_t) as a function of ϕ_e and θ_e. Since five independent variables (the electron energy, the magnitude, and the azimuthal angle of $\mathbf{q}$ and both angles of $\mathbf{p}_e$) are determined, this spectrum represents a fivefold differential cross section. On the other hand, the final-space state of the three particles is fully determined by three momentum vectors—i.e., by nine momentum components. Because of energy and momentum conversation, only five of these components are independent so that a fivefold differential cross section constitutes an FDCS. Combining $d\phi_e$ and $d\theta_e$ to the electron solid-angle differential $d\Omega_e=\sin\theta_e d\phi_e d\theta_e$ and dq and $d\phi_p$ to the projectile solid angle differential $d\Omega_p=\sin\theta_p d\phi_p dq/p_0$ (where we used that for small angles $q\approx p_0\sin\theta_p$ and $p_0\approx p_f$), we present these FDCS's as triple-differential cross sections $d^3\sigma/(d\Omega_e d\Omega_p dE_e)$. The data were normalized by setting the integral over Ω_e and Ω_p equal to the single-differential cross sections $d\sigma/dE_e$ measured for the same collision system [21].

III. THEORY

The details of the three distorted wave (3DW) approach have been given in a previous paper [22], so only the neces-

sary features will be presented here. Atomic units will be used throughout this section unless otherwise noted. The fully differential cross section is given by [23–25]

$$\frac{d^3\sigma}{d\Omega_p d\Omega_e dE_e} = N_e(2\pi)^{-5}\mu_{Ie}\mu_{\mathrm{PA}}^2\frac{k_f k_e}{k_0}|T_{fi}|^2. \tag{1}$$

The reduced mass of the helium-ion-electron subsystem is μ_{Ie}, and the reduced mass of the projectile-target atom system is μ_{PA}. The initial and final momenta of the projectile are $\mathbf{k}_0$ and $\mathbf{k}_f$, the ejected-electron's energy and momentum are given by E_e and $\mathbf{k}_e$ respectively, N_e is the number of indistinguishable electrons in the atomic shell, and all continuum waves are normalized to plane waves.

The 3DW transition matrix (T matrix) for single ionization of helium is given by [26]

$$T_{f_i} = \langle \chi_f^-|V_i|\beta_i\rangle. \tag{2}$$

Here β_i is the asymptotic form of the initial-state wave function and V_i is the initial channel interaction between the projectile and atom. The final-state distorted wave χ_f^- is an approximation to the final-state wave function which satisfies incoming-wave boundary conditions.

For heavy-particle ionization, it has been a common practice to use a semiclassical approximation assuming a straight-line trajectory for the projectile. The FDCS is then obtained from a Bessel function transform [27,28]. These approximations lead to the standard continuum distorted wave-eikonal initial state (CDW-EIS) [11,28–35], which has been very successful for less differential atomic ionization by heavy-ion impact.

We approximate the 3DW final-state wave function χ_f^- as a three-body product wave function that is given by [29,36–38]

$$\chi_f^- = \exp(i\mathbf{k}_f\cdot\mathbf{r}_a)C^-(\eta_a,\mathbf{k}_f,\mathbf{r}_a)\phi_e^-(\mathbf{k}_e,\mathbf{r}_b)C^-(\eta_{ab},\mathbf{k}_{ab},\mathbf{r}_{ab}). \tag{3}$$

Here C is the Coulomb distortion factor and the Sommerfeld parameters are given by $\eta_a = Z_P/\nu_a$ and $\eta_{ab} = -Z_P/\nu_{ab}$, $\nu_a = |\bar{\nu}_a|$, $\nu_{ab} = |\bar{\nu}_a - \bar{\nu}_b|$, and $k_{ab} = \mu_{\mathrm{pe}}\nu_{ab}$, where ν_a is the projectile velocity, ν_b the ejected electron velocity, and μ_{pe} is the reduced mass of the projectile-ejected electron subsystem ($\mu_{\mathrm{pe}} \approx 1$). The Coulomb distortion factor is

$$C^-(\eta,k,r) = \Gamma(1-i\eta)\exp(-\pi\eta/2)\ {}_1F_1(i\eta,1,-ikr-i\mathbf{k}\cdot\mathbf{r}), \tag{4}$$

where ${}_1F_1$ is a confluent hypergeometric function and Γ is the gamma function. The third two-particle wave function ϕ_e^- for the ejected-electron–helium-ion subsystem is a Hartree-Fock distorted wave [39]. It is a numerical solution of the Schrödinger equation

$$\left(-\frac{1}{2}\nabla_{r_b}^2 - U_{\mathrm{ion}}(r_b) + \frac{k_e^2}{2}\right)\phi_e^-(\mathbf{k}_e,\mathbf{r}_b) = 0, \tag{5}$$

where U_{ion} is the static Hartree-Fock potential of the helium ion. The final-state wave function χ_f^- takes all two-particle interactions into account to all orders of perturbation theory and, as a result, treats each interaction on an equal footing.

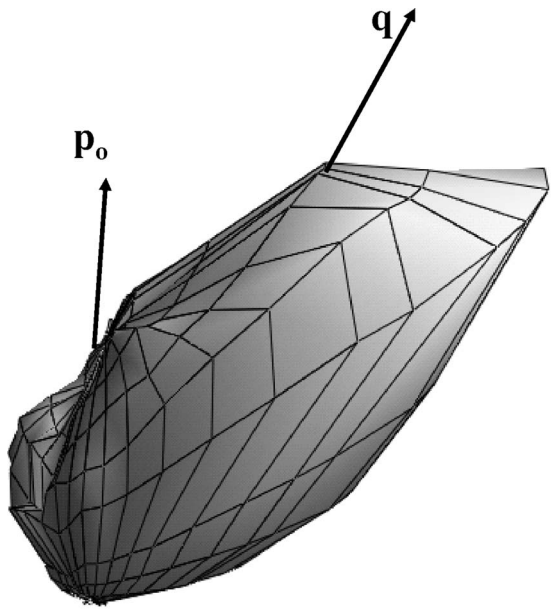

FIG. 2. Measured three-dimensional fully differential angular distribution of electrons with an energy of 5.4 eV ejected in 75-keV p+He collisions. The momentum transfer is 0.77 a.u., corresponding to a transverse momentum transfer of 0.41 a.u. The arrows labeled p_0 and q indicate the directions of the initial projectile momentum and the momentum transfer, respectively.

The unperturbed initial state in Eq. (2) is given by

$$\beta_{\mathrm{i}} = \exp(i\mathbf{k}_i\cdot\mathbf{r}_a)\psi_{1s}(\mathbf{r}_b), \tag{6}$$

where ψ_{1s} is the single-particle Hartree-Fock ground-state wave function of helium [40]. The initial wave vector for the projectile is $\mathbf{k}_i$ and the corresponding initial-channel projectile-atom interaction is

$$V_i = \frac{Z_p Z_{\mathrm{HF}}(r_a)}{r_a} - \frac{Z_p}{r_{ab}}. \tag{7}$$

Here the Hartree-Fock effective charge $Z_{\mathrm{HF}}(r_a)$ is an analytic fit to the Hartree-Fock effective charge as given by [41]. It is unity at large distances from the helium ion and approaches 2 as the projectile probes closer to the nucleus. We have evaluated the scattering amplitude of Eq. (2) by a direct six-dimensional numerical (Gauss-Legendre) quadrature as discussed by [42].

To test the importance of the final-state PI interaction on the FDCS, we have evaluated the FDCS with the PI interaction turned off (we call this calculation 2DW). The 2DW results still contain higher-order contributions involving PCI. Finally, we have calculated the FDCS within the first Born approximation (FBA) in which both the PI interaction and PCI are turned off.

IV. RESULTS AND DISCUSSION

A. Scattering plane

In Fig. 2 a three-dimensional angular distribution of ejected electrons with an energy of 5.4 eV for a transverse

momentum transfer of 0.41 a.u. is shown. The main feature in this spectrum is a pronounced peak approximately in the direction of $\mathbf{q}$. This is the behavior one would get for a pure binary interaction between the projectile and electron (i.e., if the residual ion remains completely passive). This peak is therefore traditionally called the binary peak (and we adopt this notation here), although this term is somewhat misleading. Experimentally it is not possible to distinguish whether the recoil ion was passive or not because it carried its momentum in the initial unperturbed target atom into the collision (since the unperturbed target atom is at rest and the bound electron has some momentum distribution, the residual target ion must have a momentum distribution in the initial state as well). A second structure, which is usually seen approximately in the direction of $-\mathbf{q}$ for electron and fast ion impact (at least at small η) [1,9,10], known as the recoil peak, is completely absent in our data.

In the following, we will discuss the FDCS's for different cuts through the three-dimensional angular distributions. First, we will provide a brief summary of the most important findings obtained for the data in the cut along the scattering plane which we reported earlier [19]. We will then analyze another structure found in the data, unrelated to both the binary and recoil peaks, which we only mentioned briefly in [19]. Finally, we will discuss the FDCS's for cuts along planes other than the scattering plane with some emphasis on the perpendicular plane.

In Fig. 3 we show the FDCS for electrons ejected into the scattering plane for transverse momentum transfers q_t of (from bottom to top) 0.13, 0.41, 0.73, and 1.38 a.u. The dotted vertical line at positive angles indicates the angle θ_q of $\mathbf{q}$ relative to $\mathbf{p}_0$, and the ones at negative angles indicate $-\theta_q$. In all four cases the binary peak near θ_q is clearly visible. However, a closer inspection shows that at small q_t the binary peak is shifted to larger ejection angles relative to $\mathbf{q}$. Earlier, we interpreted this backward shift relative to the beam direction as due to a higher-order process involving the PI interaction [19], which is schematically illustrated in Fig. 4. Small q_t favor relatively distant collisions, so we assume the projectile passes the target atom outside—say, on the left. In that case, the attractive interaction between the projectile and electron will scatter the projectile to the right and the projectile has an intermediate momentum p_m. The momentum transferred to the electron, $\mathbf{q}_e=\mathbf{p}_0-\mathbf{p}_m$, points to the left and in the forward direction. The projectile then gets elastically scattered by the residual target ion to the left relative to p_m because the underlying interaction is repulsive. The corresponding momentum transferred to the recoil ion $\mathbf{q}_r=\mathbf{p}_m-\mathbf{p}_f$ points to the right (the longitudinal component is negligible in elastic scattering). Since the projectile approaches the electron to a closer distance than the recoil ion, the transverse component of $\mathbf{q}_r$ is smaller than the one of $\mathbf{q}_e$. As a result, the total (measured) momentum transfer $\mathbf{q}=\mathbf{q}_r+\mathbf{q}_e$ is shifted in the forward direct relative to $\mathbf{q}_e$. Consequently, the binary peak electrons traveling in the direction of $\mathbf{q}_e$ will be observed at a larger angle than $\mathbf{q}$ (i.e., the binary peak is shifted backwards). The backwards shift of the binary peak is most pronounced at small q_t, monotonically decreases with q_t, and, in fact, eventually turns into a forward shift for $q_t=1.38$ a.u. This can be understood by keeping in mind that with increasing q_t closer collisions are favored and the probability that the projectile passes the atom on the outside, as assumed in our model, is reduced.

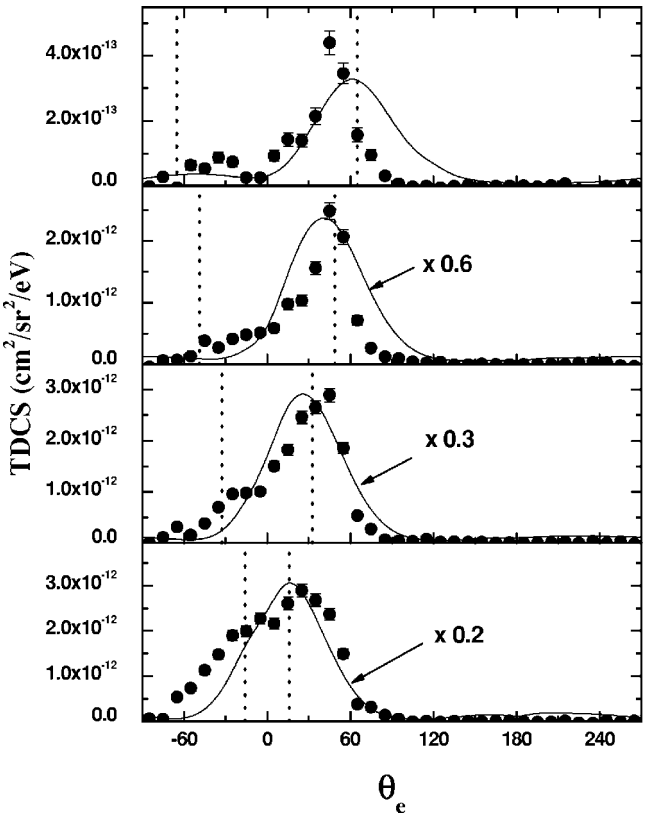

FIG. 3. Fully differential cross sections for electrons with an energy of 5.4 eV ejected into the scattering plane in 75-keV p+He collisions. The electron emission angle θ_e is defined in the text. The transverse momentum transfers are (from bottom to top) 0.13 a.u., 0.41 a.u., 0.73 a.u., and 1.38 a.u. The dotted lines indicate the angles Θ_q and $-\Theta_q$, where Θ_q is the direction of q with respect to the incident projectile direction. It is given by $\cos\Theta_q=q_z/q$. Solid lines: 3DW calculations multiplied by 0.2 (0.13 a.u.), 0.3 (0.41 a.u.), and 0.6 (0.73 a.u.), respectively.

A second structure is visible near $-\theta_q$, especially at small q_t. Again, our basic model described above offers a possible explanation for this feature as well. Now, we consider the scenario where the projectile passes the atom at relatively large distance on the right so that the electron is farther from the projectile than the residual target ion. The projectile is scattered to the left by the interaction with the electron and to the right by the interaction with the target core. However, this time the momentum transferred to the recoil ion is larger than the one transferred to the electron so that q_t points in the opposite direction as q_{et}. This is a similar behavior as in the recoil peak, but an important difference is that here the longitudinal components of $\mathbf{q}_e$ and $\mathbf{q}$ are identical (because the longitudinal momentum transfer in the elastic scattering with the target core is negligible) while in a first-order description of the recoil peak they are opposite to each other.

An alternative explanation of the structure near $-\theta_q$ is based on the PCI. Earlier, a strong peak in the forward direction observed in the FDCS's for 3.6-MeV/amu Au^{53+}+He collisions ($\eta=4.4$) was attributed to the recoil

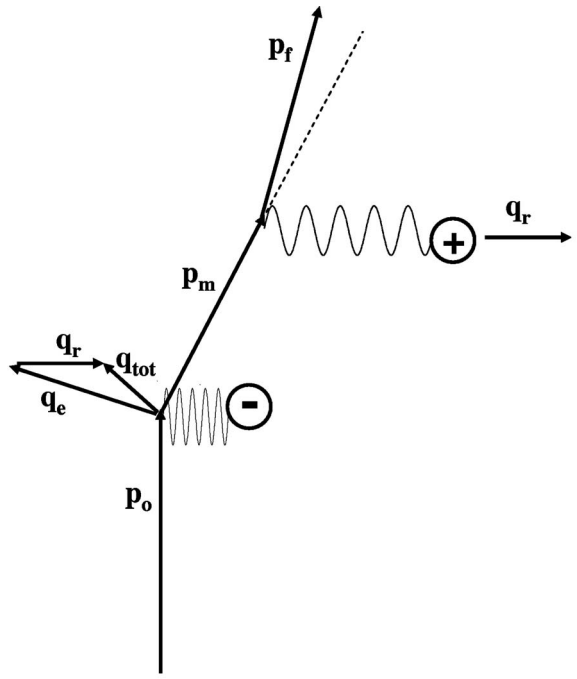

FIG. 4. Schematic diagram of the higher-order mechanism involving elastic scattering of the projectile by the residual target ion. p_0, p_m, and p_f are the initial, intermediate, and final projectile momenta, respectively, and q_e, q_r, and q are the momentum transfers to the electron and recoil ion and the total momentum transfer.

peak being strongly shifted in the forward direction by the PCI [13]. As mentioned above, we do not observe any recoil peak in the direction of $-\mathbf{q}$. However, the structure near $-\theta_q$ may also be a PCI-shifted recoil peak. It would be understandable that, in the present case, the forward shift would be much smaller than for the 3.6-MeV/amu Au^{53+} projectiles because η is much smaller. On the other hand, strong indications were found that the forward peak observed for the Au^{53+} projectiles is related to the PI interaction [18]. However, this does not rule out the earlier explanation based on the PCI. In a classical picture, the projectile and electron cannot collide consecutively without another interaction redirecting at least one of these two particles before the PCI occurs. This interaction could either be the PI interaction or the one between the electron and target ion core. Similar arguments were made by Sarkadi and Gulyas, and they referred to such mechanisms as two-center effects [43]. In this sense the explanation for the structure near $-\theta_q$ based on the PCI is just an extension of the explanation solely based on the PI interaction.

The solid curves in Fig. 3 show our 3DW calculations. The agreement with the data is not good. Neither the backward shift of the binary peak relative to the direction of $\mathbf{q}$ at small q_t nor the structures near $-\theta_q$ are reproduced. Furthermore, the absolute magnitude is off by as much as a factor of 5. Finally, with increasing q_t the width of the binary peak is increasingly overestimated by the calculation. If our interpretation of the shape of the θ dependence of the FDCS is correct, then these discrepancies show that the role of the PI interaction is severely underestimated in our theoretical model. The same conclusion was also drawn from a comparison between experiment and theory for very fast highly charged ion impact [12]. On the other hand, it is currently not clear to what extent the differences in magnitude can be attributed to the PI interaction. We have recently shown that the magnitude can be extremely sensitive to the description of the interaction between the active (ejected) and passive electron which remains bound in the ground state of the target core ion. Depending on the specific description of that interaction, very good agreement in magnitude can be achieved even without incorporating the PI interaction [44].

B. Out-of-plane electron ejection

In the scattering plane effects due to the PI interaction are usually not as pronounced as those reported here, except for extremely large η [18]. For relativistic ion impact at an η comparable to the present collision system some contributions of the PI interaction in the scattering plane were identified, which were, however, more of a quantitative nature [45]. Generally, the relative importance of such effects tends to strongly increase as the direction of the electron ejection departs from the scattering plane [12]. In the following we therefore analyze the role of the PI interaction for out-of-plane electron ejection.

First, we will discuss the shape of the three-dimensional FDCS as a function of q_t. For simplicity, in the following the term recoil peak refers to any structure centered on $-\mathrm{q}_t$—i.e., to both the conventional recoil peak and to the structure we observe near $-\theta_q$. We start the analysis by plotting in Fig. 5 the FDCS of Fig. 2 from a different perspective, viewing it from the back in the beam direction. In this figure $\mathbf{q}_t$ is pointing horizontally to the right; i.e., the scattering plane is oriented along the horizontal and the perpendicular plane is oriented along the vertical. The bottom of Fig. 5 shows these cross sections from the same perspective calculated with the FBA. The comparison between the measured and calculated data looks similar to what was observed for 100-MeV/amu C^{6+}+He [12] and 1-GeV/amu U^{92+}+He collisions [46]: while in the calculation there is a minimum along the perpendicular plane separating the binary peak from the recoil peak, in the experimental FDCS such minima are not present at all. In fact, the minimum in the FBA is much stronger than it appears in this particular perspective. Because $\mathbf{q}$—and therefore the binary peak—is pointing in the forward direction and the recoil peak in the backward direction, the cross section in these peaks "in front" and "behind" the minimum give the false impression that the minimum is filled up. In contrast, even without this artifact due to the perspective, there is no minimum in the data, as can be seen from Fig. 2.

To analyze the shape of the FDCS in the region of the minimum predicted by the FBA more systematically, we determined the ratio R of the integrated counts in the semiplane perpendicular to the scattering plane divided by the integrated counts in the semiscattering plane containing $-\mathbf{q}_t$. This ratio is plotted in Fig. 6 as a function of q_t. R is a crude measure for the shape of the azimuthal angular dependence of the FDCS. A minimum separating the recoil peak from the binary peak corresponds to a relatively small value of R and an increasing R signifies an increasing filling of such a mini-

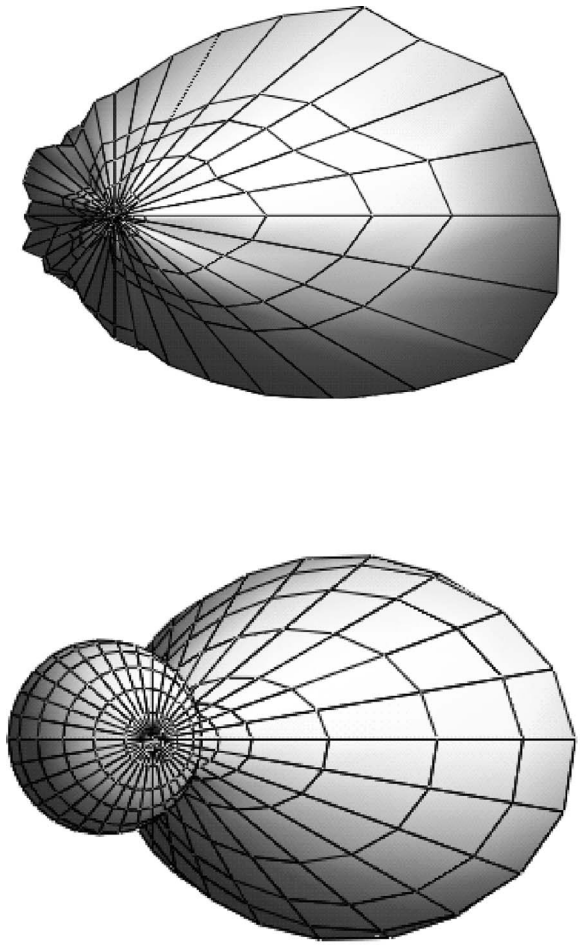

FIG. 5. Three-dimensional FDCS of Fig. 2 viewed in the beam direction (top). The bottom part shows these FDCS calculated within the FBA.

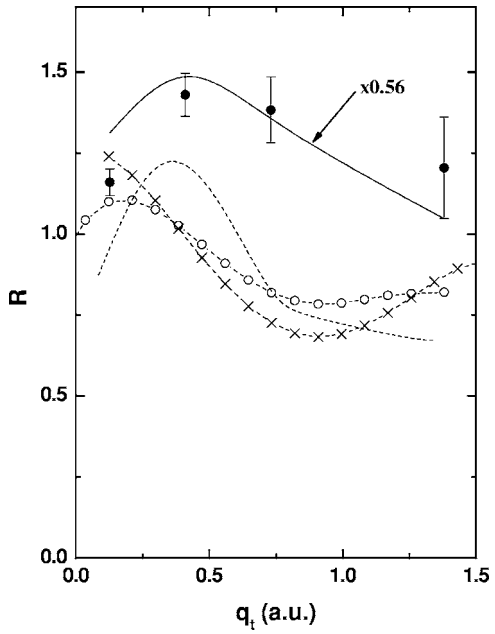

FIG. 6. Ratio R between the integrated counts in one of the perpendicular semiplanes to the integrated counts in the semiscattering plane containing $-\mathbf{q}_t$ as a function of q_t. Solid curve: simple classical model based on Rutherford scattering (see text). Dashed curve with circles: FBA. Dashed curve with crosses: 2DW. Dashed curve: 3DW.

mum. In the data, $R>1$ for all q_t and there is a maximum at about $q_t=0.5$ a.u. This dependence of R on q_t is very similar to the one we obtained earlier for 1-GeV/amu U^{92+}+He collisions [46].

In the following we will analyze the extent to which the q_t dependence of R in the data can be explained in terms of a higher-order mechanism involving the PI interaction. To this end we employ a simple classical model to describe elastic scattering between the projectile and target-ion core in terms of Rutherford scattering. In our model we make the following approximations: (i) The potential between the projectile and the target-ion core is assumed to be Coulombic. (ii) We treat the elastic scattering as independent of the projectile-electron interaction leading to the electron ejection. (iii) We neglect the initial momentum distribution of the electrons in the ground state of He.

Using the first approximation, the elastic scattering cross section (in a.u.) can be expressed as $d\sigma/dq_r=8\pi\eta^2Z_t^2/q_{rt}^3$, where q_{rt} is the transverse component of the momentum transferred only to the recoil ion (the longitudinal momentum is essentially 0) and Z_t is the effective target atomic number. We can express q_{rt} in terms of q_t and the transverse component of the momentum transfer only to the electron (occurring in the preceding projectile-electron interaction) q_{et}. Using the collision geometry, which is shown in Fig. 7, and the law of cosines, we get $q_{rt}=(q_t^2+q_{et}^2-2q_tq_{et}\cos\phi)^{1/2}$ because $\mathbf{q}_t=\mathbf{q}_{et}+\mathbf{q}_{rt}$. The angle ϕ enclosed by $\mathbf{q}_t$ and $\mathbf{q}_{et}$ is 90° for electron ejection into the perpendicular semiplane and 180° for ejection into the semiplane containing $-\mathbf{q}_t$. Within the second approximation, R can be expressed as the ratio between the elastic scattering cross sections at these two angles, because if the ionization probability is independent of the elastic scattering, it divides out in this ratio. Substituting the expression for q_{rt} found

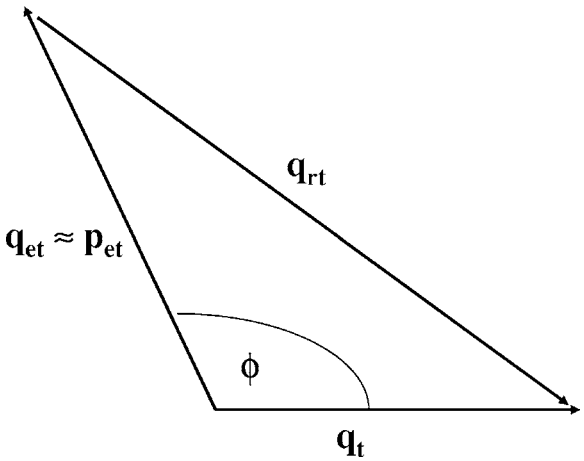

FIG. 7. Vector diagram of the transverse momentum transfers to the electron q_{et} and to the recoil ion q_{rt} and total transverse momentum transfer q_t. The angle ϕ between q_{et} and q_t is 90° for the perpendicular semiplane and 180° for the semiscattering plane containing $-\mathbf{q}_t$.

above in $R=d\sigma/dq_{rt}(\phi=90°)/d\sigma/dq_{rt}(\phi=180°)$ yields $R=[(q_t+q_{et})^2/(q_t^2+q_{et}^2)]^{3/2}$. Finally, using the third approximation we can equate q_{et} to the transverse electron momentum p_{et}, for which we used an average value obtained from the measured electron momentum distribution for each q_t. The q_t dependence of R resulting from this simple, classical model is shown as the solid curve in Fig. 6. For comparison in shape, we divided the calculated values by 1.8, which shows that there is a significant difference in magnitude as compared to the experimental data. However, the shape of the q_t dependence of the measured R is well reproduced. It is interesting to note that the overall difference in magnitude is exactly the same as found for 1-GeV/amu U^{92+}+He collisions [46].

The dashed curve with circles shows R calculated within the FBA. Not surprisingly, it is in poor agreement with the data. Although there is a maximum, it occurs at much smaller q_t than found in the data. Furthermore, it should be noted that for 1 GeV/amu U^{92+}+He collisions, where the measured data of R look essentially identical to the present experimental results, the FBA has no maximum at all and asymptotically goes to 0 as q_t becomes infinitesimally small (when q_t equals exactly 0, R has to jump to 1 because no plane is defined). Therefore, as expected for this relatively large value of η, R is strongly influenced by higher-order effects. One important goal of this work is to find out which specific higher-order mechanism is responsible for the features observed in R. The higher-order interactions contained in the theory are PCI (projectile and electron) and PI (projectile and ion). As mentioned in Sec. III, the 3DW contains all these higher-order interactions and the 2DW contains only PCI.

The dashed curve with crosses shows the results of the 2DW calculation, which does not include the PI interaction. Amazingly, the disagreement with the data gets even worse than for the FBA, both in shape and in magnitude. Instead of a maximum, we now obtain a minimum at about 0.8 a.u. and the measured ratios are generally considerably underestimated. The dashed curve shows R calculated with our 3DW model, which includes all higher-order two-particle interactions in the final state. The agreement in shape for the q_t dependence of R with the data is significantly improved compared to the FBA and 2DW calculations. More specifically, the 3DW calculation seems to reproduce the position of the maximum fairly well. However, there are still considerable discrepancies in magnitude. Nevertheless, overall the comparison between the data and the various calculations seems to support our above conclusion that the q_t dependence of R is mostly determined by a higher-order mechanism involving the PI interaction.

A further test of the description of higher-order contributions in theory is provided by the θ_e dependence of the FDCS in the perpendicular plane. As mentioned above, signatures of the PI interaction are observed in the scattering plane. Such effects should be even more pronounced in the perpendicular plane. Because of momentum conservation, a first-order ionization process can only eject the electron out of the scattering plane if the electron had, at the instant of the primary interaction with the projectile, a momentum component outside the scattering plane already in the initial bound state

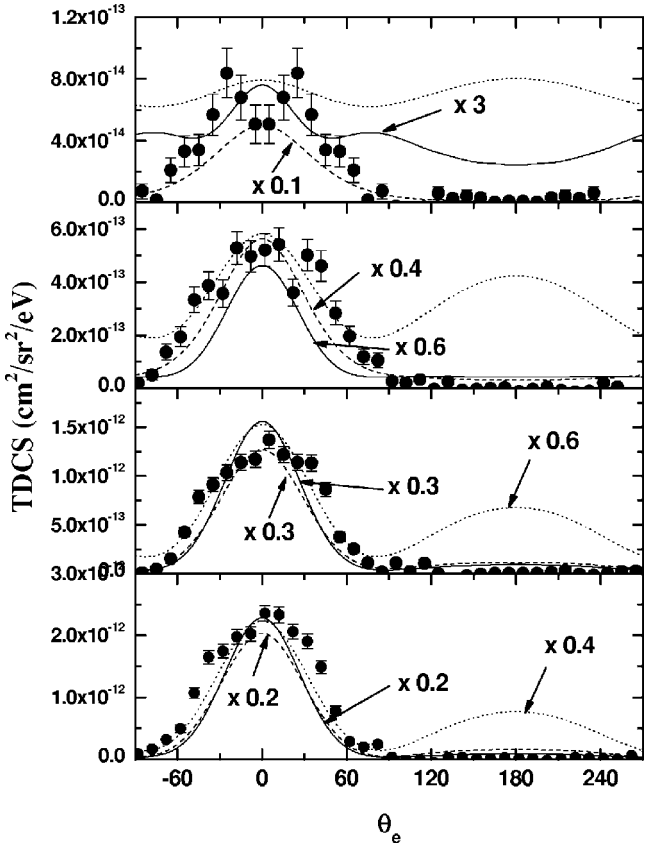

FIG. 8. Fully differential cross sections for electrons with an energy of 5.4 eV ejected into the perpendicular plane in 75-keV p+He collisions. The transverse momentum transfers are (from bottom to top) 0.13 a.u., 0.41 a.u., 0.73 a.u., and 1.38 a.u. Solid lines: 3DW calculations multiplied by 0.2 (0.13 a.u.), 0.3 (0.41 a.u.), 0.6 (0.73 a.u.), and 3 (1.38 a.u.), respectively. Dashed lines: 2DW calculations multiplied by 0.2 (0.13 a.u.), 0.3 (0.41 a.u.), 0.4(0.73 a.u.), and 0.1 (1.38 a.u.) respectively. Dotted lines: FBA multiplied by 0.4 (0.13 a.u.) and 0.6 (0.41 a.u.), respectively.

of the target atom. Therefore, the relative importance of higher-order contributions tends to increase with increasing departure from the scattering plane.

The measured FDCS's for the perpendicular plane are plotted as a function of θ_e in Fig. 8 for the same q_t as the FDCS's for the scattering plane of Fig. 3. Except for $q_t=1.38$ a.u., the FDCS's exhibit a strong peak at $\theta_e=0$. With increasing q_t this maximum becomes increasingly broader and eventually separates into two peaks at about $\theta_e=\pm 30°$ for the largest q_t leaving a minimum at $\theta_e=0$. The maxima at $\theta_e=0$ for small q_t are actually expected even within a first-order description. In any first-order Born treatment the FDCS's must be cylindrically symmetric about $\mathbf{q}$. As a result, if the electron is initially bound in a $1s$ state, maxima cannot occur at angles other than 0 and 180° in the perpendicular plane. For the small q_t, we observe peak structures in the forward rather than in the backward direction because $\mathbf{q}$ points strongly in the forward direction. On the other hand, the maxima at $\theta_c=\pm 30°$ for $q_t=1.38$ a.u. break the cylindrical symmetry about $\mathbf{q}$ and are therefore another clear signature of higher-order effects.

Once again, we will attempt to shed some light on the specific higher-order mechanism giving rise to the features observed in the data by comparing to calculations successively incorporating the various higher-order interactions. The dotted curve in Fig. 8 shows our FBA results, the dashed curve the 2DW calculations, and the solid curve the 3DW calculations. Except for the largest q_t, the FBA reproduces the shape of the maximum at 0° fairly well. However, it predicts a second pronounced peak at 180°, which is not present at all in the data. Furthermore, there is significant disagreement in magnitude. Most noticeably, at $q_t=1.38$ a.u. the FBA does not even remotely resemble the experimental data. Some improved agreement with the data is achieved with the 2DW calculation to the extent that the peak at 180° for small q_t is reduced to a small residue which is barely visible on the scale of Fig. 8 and it is completely absent for large q_t. On the other hand, there is no improved agreement in the absolute magnitude and, in fact, at 0° the discrepancy is even much larger than for the FBA. Most importantly, for $q_t=1.38$ a.u., like the FBA the 2DW calculation also does not provide the slightest indication for a maximum at angles other than 0 and 180°.

Finally, although significant improvement with the data is achieved with the full 3DW calculation, major discrepancies remain. On the positive side, the 3DW calculation removes the residues of the peak at 180° which are still visible in the 2DW results. Furthermore, peak structures are now seen at angles other than 0 and 180°. On the negative side, however, these maxima occur at very different angles ($\approx \pm 80°$) and are significantly less pronounced than in the data. Furthermore, overall there is no improved agreement in magnitude compared to the 2DW calculation and even worse agreement compared to the FBA results. Finally, for angles $|\theta_e| > 60°$ at $q_t=1.38$ a.u. the FDCS's are overestimated by an order of magnitude. Nevertheless, in spite of these problems the comparison between the 2DW and 3DW calculations shows that the PI interaction is capable of producing peak structures at angles other than 0 and 180°. At the same time, the comparison between the 2DW and FBA results suggests that such structures are not generated by PCI or the final-state interaction between the electron and residual target ion. We take this as another, although admittedly not a conclusive, indication that the features observed in the measured FDCS's are to a large extent due to the PI interaction. However, the description of this interaction in the 3DW approach is evidently rather incomplete.

V. CONCLUSIONS

We have reported complete three-dimensional images of measured FDCS's for single ionization in 75-keV p+He collisions. For such collision systems, involving light ionic projectiles at intermediate energies, neither measured nor calculated FDCS's were available until we reported the first results last year [19]. We found features in the data which were not observed in previous experiments studying the FDCS's for high-energy ion impact or electron impact. For example, in the present experimental results the binary peak is shifted in the backwards direction relative to the direction of $\mathbf{q}$ for small q_t. In Ref. [19] we readily showed that such a backward shift is not observable for energetic ion impact. Furthermore, a new structure was found in the scattering plane at approximately $\theta_e=-\theta_q$. We have argued that both the backwards shift of the binary peak and the structure near $-\theta_q$ are due to a higher-order mechanism involving the PI interaction.

We also analyzed the projection of the three-dimensional FDCS's onto the azimuthal plane. Here, the minimum between the binary and recoil peaks predicted by the FBA is completely absent in the data. In the ratio R of the integrated counts in the semiplane perpendicular to the scattering plane to the integrated counts in the semiscattering plane containing $-\mathbf{q}_t$ as a function of q_t, we find a maximum at about 0.5 a.u. The features observed in this projection are qualitatively consistent with a simple model which describes the PI interaction in terms of classical Rutherford scattering. Finally, in the angular dependence of the perpendicular plane we observe a peak structure at about 30° for large q_t, which we also attribute to the PI interaction.

Our theoretical results are very sensitive to the specific description of high-order interactions, especially outside the scattering plane. For example, if only higher-order effects in the projectile-electron interaction are accounted for, the calculated q_t dependence of R bares no resemblance to the experimental data at all. On the other hand, if the PI interaction is incorporated on top of the PCI, reasonable qualitative agreement is achieved. Furthermore, at large q_t a peak structure is obtained in the perpendicular plane at an angle where for symmetry reasons no peak structure can occur for a He target in a first-order treatment (between 0 and 180°), again in qualitative agreement with the data. However, even the full 3DW calculation exhibits significant discrepancies with the data, both in shape and in magnitude. The comparison between experiment and the various theoretical models supports our conclusion that the features observed in the data are to a large extent due to the PI interaction. But it also shows that the description of that interaction is still rather incomplete.

Since the first three-dimensional FDCS's were published [12], such data were reported for a large variety of collisions systems ([9,10] and references therein) including electron impact. Evidence is accumulating that the unexpected, and until now not fully understood, features can be traced to the PI interaction. In fact, it seems to play an even more important role than the PCI, which previously was assumed to be the dominant higher-order effect at large perturbation [21,47,48] (except for relativistic projectiles).

ACKNOWLEDGMENTS

Funding from the National Science Foundation under Grants Nos. PHY-0353532 and PHY-0070872 is gratefully acknowledged.

[1] H. Ehrhardt, K. Jung, G. Knoth, and P. Schlemmer, Z. Phys. D: At., Mol. Clusters **1**, 3 (1986) and references therein.
[2] H. Ehrhardt, M. Schulz, T. Tekaat, and K. Willmann, Phys. Rev. Lett. **22**, 89 (1969).
[3] P. Marchalant, C. T. Whelan, and H. R. J. Walters, J. Phys. B **31**, 1141 (1998).
[4] T. N. Rescigno, M. Baertschy, W. A. Isaacs, and C. W. McCurdy, Science **286**, 2474 (1999).
[5] M. Dürr, C. Dimopoulou, B. Najjari, A. Dorn, and J. Ullrich (unpublished).
[6] R. W. van Boeyen, N. Watanabe, J. W. Cooper, J. P. Doering, J. H. Moore, and M. A. Coplan, Phys. Rev. A **73**, 032703 (2006).
[7] A. J. Murray, M. B. J. Woolf, and F. H. Read, J. Phys. B **25**, 3021 (1992).
[8] M. Schulz, R. Moshammer, D. H. Madison, R. E. Olson, P. Marchalant, C. T. Whelan, S. Jones, M. Foster, H. Kollmus, A. Cassimi, and J. Ullrich, J. Phys. B **34**, L305 (2001).
[9] M. Schulz, R. Moshammer, D. Fischer, D. H. Madison, A. Hasan, N. V. Maydanyuk, and J. Ullrich, Mater. Sci. Res. Int. **5**, 679 (2004).
[10] M. Schulz, R. Moshammer, D. Fischer, A. Hasan, N. V. Maydanyuk, and J. Ullrich, *Atomic processes in plasmas*, edited by J. Cohen and S. Mazevet, AIP Conf. Proc. **730**, 35 (2004).
[11] D. Madison, M. Schulz, S. Jones, M. Foster, R. Moshammer, and J. Ullrich, J. Phys. B **35**, 3297 (2002).
[12] M. Schulz, R. Moshammer, D. Fischer, H. Kollmus, D. H. Madison, S. Jones, and J. Ullrich, Nature (London) **422**, 48 (2003).
[13] M. Schulz, R. Moshammer, A. N. Perumal, and J. Ullrich, J. Phys. B **35**, L161 (2002).
[14] D. Fischer, R. Moshammer, M. Schulz, A. Voitkiv, and J. Ullrich, J. Phys. B **35**, 3555 (2003).
[15] M. Foster, D. H. Madison, M. Schulz, S. Jones, and J. Ullrich, J. Phys. B **37**, 3797 (2004).
[16] R. T. Pedlow, S. F. C. O'Rourke, and D. S. F. Crothers, Phys. Rev. A **72**, 062719 (2005).
[17] M. F. Ciappina and W. R. Cravero, J. Phys. B **39**, 1091 (2006).
[18] M. Schulz, R. Moshammer, D. Fischer, and J. Ullrich, J. Phys. B **36**, L311 (2003).
[19] N. V. Maydanyuk, A. Hasan, M. Foster, B. Tooke, E. Nanni, D. H. Madison, and M. Schulz, Phys. Rev. Lett. **94**, 243201 (2005).
[20] A. D. Gaus, W. Htwe, J. A. Brand, T. J. Gay, and M. Schulz, Rev. Sci. Instrum. **65**, 3739 (1994).
[21] M. Schulz, T. Vajnai, A. D. Gaus, W. Htwe, D. H. Madison, and R. E. Olson, Phys. Rev. A **54**, 2951 (1996).
[22] M. Foster, D. H. Madison, J. L. Peacher, M. Schulz, S. Jones, D. Fischer, R. Moshammer, and J. Ullrich, J. Phys. B **37**, 1565 (2004).
[23] J. Berakdar, J. S. Briggs, and H. Klar, J. Phys. B **26**, 285 (1993).
[24] H. Bethe, Ann. Phys. (Leipzig) **5**, 325 (1930).
[25] M. Inokuti, Rev. Mod. Phys. **43**, 297 (1971).
[26] M. Gell-Mann and M. L. Goldberger, Phys. Rev. **91**, 398 (1953).
[27] L. Wilets and S. J. Wallace, Phys. Rev. **169**, 84 (1968).
[28] D. S. F. Crothers and L. J. Dubé, Adv. At., Mol., Opt. Phys. **30**, 287 (1993).
[29] D. S. F. Crothers and J. F. McCann, J. Phys. B **16**, 3229 (1983).
[30] X. Fang and J. F. Reading, Nucl. Instrum. Methods Phys. Res. B **53**, 453 (1991).
[31] H. Fukuda, I. Shimamura, L. Vegh, and T. Watanabe, Phys. Rev. A **44**, 1565 (1991).
[32] H. Fukuda, T. Watanabe, I. Shimamura, and L. Vegh, Nucl. Instrum. Methods Phys. Res. B **53**, 410 (1991).
[33] V. D. Rodríguez and R. O. Barrachina, Phys. Rev. A **57**, 215 (1998).
[34] R. Moshammer, A. N. Perumal, M. Schulz, V. D. Rodriguez, H. Kollmus, R. Mann, S. Hagmann, and J. Ullrich, Phys. Rev. Lett. **87**, 223201 (2001).
[35] J. Fiol, V. D. Rodríguez, and R. O. Barrachina, J. Phys. B **34**, 933 (2001).
[36] P. J. Redmond (unpublished), as discussed in L. Rosenberg, Phys. Rev. D **8**, 1833 (1973).
[37] C. R. Garibotti and J. E. Miraglia, Phys. Rev. A **21**, 572 (1980).
[38] M. Brauner, J. S. Briggs, and H. Klar, J. Phys. B **22**, 2265 (1989).
[39] S. Jones and D. H. Madison, J. Phys. B **27**, 1423 (1993).
[40] F. W. Byron and C. J. Joachain, Phys. Rev. **146**, 1 (1966).
[41] R. H. Garvey, C. H. Jackman, and A. E. S. Green, Phys. Rev. A **12**, 1144 (1975).
[42] S. Jones and D. H. Madison, Phys. Rev. Lett. **81**, 2886 (1998).
[43] L. Sarkadi, L. Gulyás, and L. Lugosi, Phys. Rev. A **65**, 052715 (2002).
[44] M. Foster, J. L. Peacher, M. Schulz, A. Hasan, and D. H. Madison, Phys. Rev. A **72**, 062708 (2005).
[45] A. B. Voitkiv, B. Najjari, R. Moshammer, M. Schulz, and J. Ullrich, J. Phys. B **37**, L365 (2004).
[46] M. Schulz, R. Moshammer, A. Voitkiv, B. Najjari, and J. Ullrich, Nucl. Instrum. Methods Phys. Res. B **235**, 296 (2005).
[47] R. Moshammer, J. Ullrich, M. Unverzagt, W. Schmilt, P. Jardin, R. E. Olson, R. Mann, R. Dörner, V. Mergel, U. Buck, and H. Schmidt-Böcking, Phys. Rev. Lett. **73**, 3371 (1994).
[48] L. An, K. Khayyat and M. Schulz, Phys. Rev. A **63**, 030703(R) (2001).